

# On the Origin of Dark Current in Organic Photodiodes

Giulio Simone, Matthew J. Dyson, Christ H. L. Weijtens, Stefan C. J. Meskers, Reinder Coehoorn, René A. J. Janssen,\* and Gerwin H. Gelinck\*

**Minimizing the reverse bias dark current while retaining external quantum efficiency is crucial if the light detection sensitivity of organic photodiodes (OPDs) is to compete with inorganic photodetectors. However, a quantitative relationship between the magnitude of the dark current density under reverse bias ( $J_d$ ) and the properties of the bulk heterojunction (BHJ) active layer has so far not been established. Here, a systematic analysis of  $J_d$  in state-of-the-art BHJ OPDs using five polymers with a range of energy levels and charge transport characteristics is presented. The magnitude and activation energy of  $J_d$  are explained using a model that assumes charge injection from the metal contacts into an energetically disordered semiconductor. By relating  $J_d$  to material parameters, insights into the origin of  $J_d$  are obtained that enable the future selection of successful OPD materials.**

Solution processed organic photodiodes (OPDs) are attracting attention for use as photodetectors since they possess several advantages over their inorganic counterparts. These include a higher absorption coefficient, greater color selectivity, and compatibility with low temperature solution processing that enables cost-effective, large-area image detectors.<sup>[1–3]</sup> The bulk heterojunction (BHJ) architecture, comprising a phase-separated blend of a donor polymer and a fullerene acceptor sandwiched between charge extraction layers, is widely employed<sup>[4–6]</sup> to enhance photocarrier generation at the donor–acceptor interface and charge extraction via bicontinuous

percolating networks. Whereas OPDs operate under forward bias in photovoltaic mode for power conversion, they typically operate under reverse bias for light detection. The all-important light sensitivity is widely parameterized by the specific detectivity, defined as

$$D^* = \frac{R\sqrt{AB}}{i_{\text{noise}}} \quad (1)$$

where  $R$  is the spectral responsivity in  $\text{A W}^{-1}$ ,  $A$  is the device active area in  $\text{m}^2$ ,  $B$  is the detection band width in Hz, and  $i_{\text{noise}}$  is the noise current in A.<sup>[1,7]</sup> An important contribution to  $i_{\text{noise}}$  is the dark current density ( $J_d$ ), which can span multiple orders of magnitude depending on

the material properties and device architecture.<sup>[2,4]</sup> Since minimizing  $J_d$  while maintaining a high responsivity is a prerequisite for high detectivity OPDs, an enhanced understanding of the mechanism that determines  $J_d$  can thus direct further detectivity improvement strategies.


The intrinsic dark current of OPDs is typically attributed to either charge carrier injection from the metal contacts into the organic semiconductor<sup>[4,5,8]</sup> or to bulk thermal generation within the active layer.<sup>[9,10]</sup> Whereas thermal generation typically makes a limited contribution to  $J_d$  as organic materials have a relatively large bandgap ( $>1$  eV),<sup>[2]</sup> charge injection may not be negligible under an applied reverse bias voltage. As such, modifying the metal-semiconductor interfaces by introducing electron and hole blocking layers (EBLs and HBLs) to suppress charge injection is a common strategy to reduce  $J_d$ ,<sup>[5,11,12]</sup> along with increasing the active layer thickness.<sup>[13]</sup> Photomultiplication is another strategy to enhance OPD performance.<sup>[14–16]</sup> However, despite the importance of  $J_d$ , a quantitative relation between its magnitude and BHJ properties, such as the energetic landscape and charge transport characteristics, remains unestablished. This study aims to clarify the relationship between  $J_d$  and the properties of the organic semiconductor blend, with a view to providing material selection guidelines to improve BHJ OPD sensitivity.

Herein, we investigate  $J_d$  in BHJ OPDs based on five different polymer donors with widely varying optical bandgaps, each combined with a common fullerene acceptor. The active layer thickness ( $\approx 280$  nm) and the contact layers are kept the same in all OPDs. We show that at  $-2$  V reverse bias,  $J_d$  depends substantially on the polymer donor, differing by five orders of magnitude. Furthermore, for the OPDs analyzed in this work the current density, measured in the dark at  $-2$  V, correlates exponentially with the open-circuit voltage ( $V_{\text{oc}}$ ) measured under a simulated solar spectrum. This suggests that  $J_d$

G. Simone, Dr. M. J. Dyson, Dr. C. H. L. Weijtens, Dr. S. C. J. Meskers, Prof. R. Coehoorn, Prof. R. A. J. Janssen, Prof. G. H. Gelinck  
Molecular Materials and Nanosystems  
Institute of Complex Molecular Systems  
Eindhoven University of Technology  
P.O. Box 513, 5600 MB Eindhoven, The Netherlands  
E-mail: r.a.j.janssen@tue.nl; g.h.gelinck@tue.nl

Prof. R. A. J. Janssen  
Dutch Institute for Fundamental Energy Research  
De Zaale 20, 5612 AJ Eindhoven, The Netherlands

Prof. G. H. Gelinck  
Holst Centre  
TNO-The Dutch Organization for Applied Scientific Research  
High Tech Campus 31, 5656 AE Eindhoven, The Netherlands

 The ORCID identification number(s) for the author(s) of this article can be found under <https://doi.org/10.1002/adom.201901568>.

© 2019 The Authors. Published by WILEY-VCH Verlag GmbH & Co. KGaA, Weinheim. This is an open access article under the terms of the Creative Commons Attribution-NonCommercial License, which permits use, distribution and reproduction in any medium, provided the original work is properly cited and is not used for commercial purposes.

DOI: 10.1002/adom.201901568

depends on the effective bandgap, defined as the energy difference between the lowest unoccupied molecular orbital (LUMO) of the acceptor and the highest occupied molecular orbital (HOMO) of the donor. However, we counterintuitively find that the thermal activation energy of  $J_d$  ( $\approx 0.25$  eV) is much lower than expected from the acceptor LUMO–donor HOMO energy difference and nearly independent of the donor polymer. To rationalize these findings, we propose a simple model based on charge injection from the contacts into an energetically disordered semiconductor that explains the  $J_d$  magnitude and thermal activation energy for all donor polymers.

We fabricated solution-processed OPDs based on five polymer:fullerene BHJs, specifically poly[[4-(2-ethylhexyl)-4H-dithieno[3,2-*b*:2',3'-*d*]pyrrole-2,6-diyl]-2,5-selenophenediyl[2,5-bis(2-ethylhexyl)-2,3,5,6-tetrahydro-3,6-dioxopyrrolo[3,4-*c*]pyrrole-1,4-diyl]-2,5-selenophenediyl] (PDPPSDTSPS), poly[[2,5-bis(2-hexyldecyl)-2,3,5,6-tetrahydro-3,6-dioxopyrrolo[3,4-*c*]pyrrole-1,4-diyl](3''',4'-dihexyl[2,2':5'',2'':5''',2''':5''',2''':5'''-quinquethiophene]-5,5'''-diyl)] (PDPP5T), poly[[2,5-bis(2-hexyldecyl)-2,3,5,6-tetrahydro-3,6-dioxopyrrolo[3,4-*c*]pyrrole-1,4-diyl]-alt-[2,2':5',2'':terthiophene]-5,5''-diyl] (PDPP3T), poly[2-methoxy-5-(3',7'-dimethyloctyloxy)-1,4-phenylenevinylene]

(OC<sub>1</sub>C<sub>10</sub>-PPV), and poly[*N*-9''-hepta-decanyl-2,7-carbazole-alt-5,5-(4',7'-di-2-thienyl-2',1',3'-benzothiadiazole)] (PCDTBT), each blended with phenyl-C<sub>61</sub>-butyric acid methyl ester (PC<sub>61</sub>BM). The chemical structures are displayed in Figure 1a. To determine the energy levels in the BHJ that define the effective bandgap, we measured the HOMO energies of PDPP5T, PDPP3T, OC<sub>1</sub>C<sub>10</sub>-PPV, and PCDTBT (Figure 1b) by ultraviolet photoelectron spectroscopy (UPS) (Figure S1, Supporting Information). The HOMO of PDPPSDTSPS was taken from ref. [17]. The LUMO of PC<sub>61</sub>BM was taken from ref. [18] and was measured with low-energy inverse photoelectron spectroscopy (LEIPS).

All OPDs investigated comprise a Mo/MoO<sub>x</sub> bottom contact and a semi-transparent LiF (1 nm)/Al (1.5 nm)/Ag (10 nm)/ZnS (30 nm) top contact to extract under reverse bias the photogenerated holes and electrons, respectively. Considering the top electrode, LiF/Al creates a low work function contact, the Ag layer ensures good lateral conductivity, and the ZnS layer is used as a dielectric to improve light in-coupling. The OPD architecture is shown in Figure S2, Supporting Information. The conditions for depositing the BHJ layers (see the Experimental Section) have been previously optimized to achieve optimal

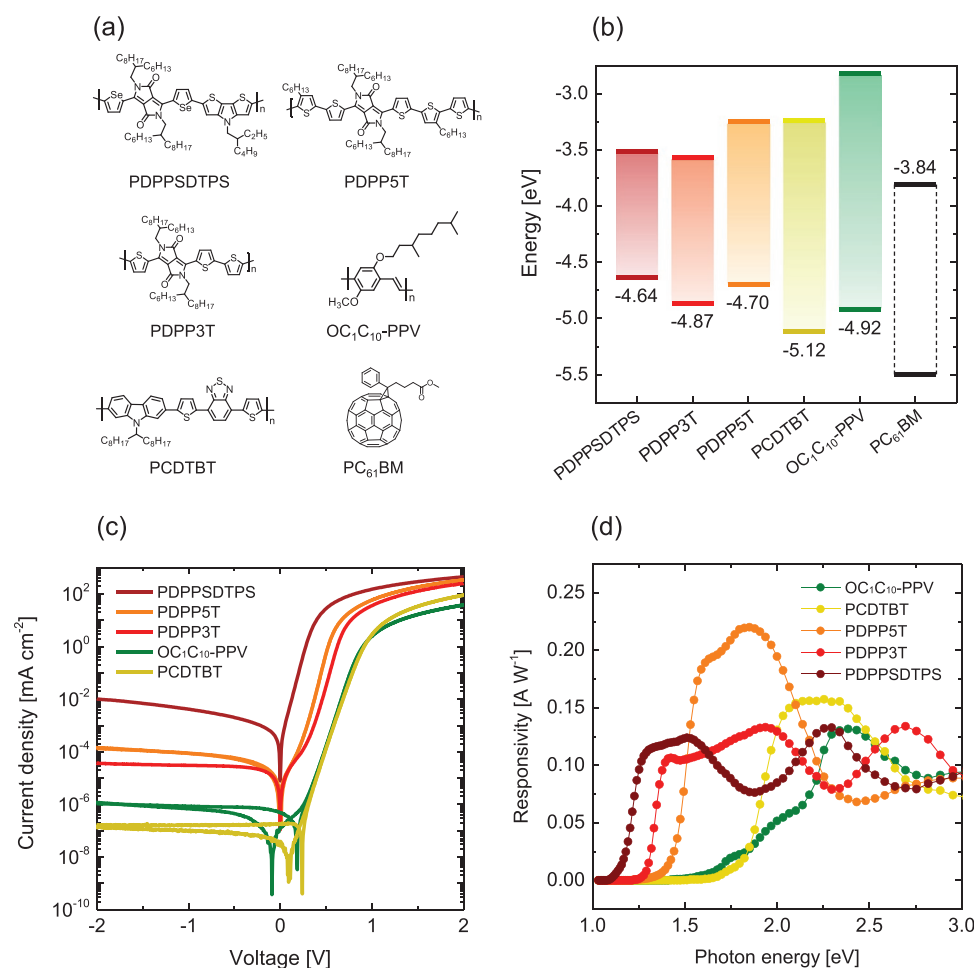


**Figure 1.** a) Chemical structures of the donor polymers and the fullerene derivative acceptor (PC<sub>61</sub>BM). b) HOMO levels of all polymers, LUMO level of PC<sub>61</sub>BM, and the corresponding optical bandgaps. c) Current density–voltage characteristics in dark conditions for BHJ OPDs with different polymers.  $J_d$  at  $V = -2$  V varies by nearly five orders of magnitude depending on the polymer, despite the same active layer thickness. d) Responsivity spectra at  $V = -2$  V.

BHJ morphologies with maximal photocurrent response.<sup>[19–23]</sup> PDPPSDTPS, PDPP5T, and PDPP3T blends with PC<sub>61</sub>BM have an optimal polymer to fullerene weight ratio of 1:2 while for OC<sub>1</sub>C<sub>10</sub>-PPV and PCDTBT this ratio is 1:4. In the optimized blends both components are well-mixed in all directions and the dimensions of phase separated domains are typically less than 20 nm. Both components contact both electrodes and percolating pathways for holes and electrons exist throughout the film. Importantly, the photoactive layer thickness was kept the same ( $\approx 280$  nm) in all OPDs, thereby ensuring the same effective electric field under a given applied voltage.

The dark current density–voltage ( $J$ – $V$ ) characteristics are shown in Figure 1c for all OPDs.  $J_d$  at  $-2$  V varies by nearly five orders of magnitude depending on the polymer. It has previously been shown that extrinsic shunt paths caused by substrate defects, dust particles, or localized fluctuations in material properties can result in local increases in leakage currents and thus random variations in  $J_d$  amongst nominally identical devices.<sup>[24,25]</sup> By using relatively thick semiconductor layers ( $\approx 280$  nm) such effects are reduced, leading to  $J_d$  variation ( $-2$  V) of less than a factor of 2 within device batches (Figure S3, Supporting Information). Although extrinsic shunt paths cannot be completely ruled out in these OPDs, their existence cannot explain the five orders of magnitude difference in  $J_d$  across five different donor:acceptor blends given the comparatively minor intra-batch variation. Thus, we attribute the differences in  $J_d$  listed in Table 1 to the intrinsic properties of the BHJ layers, specifically the energetic landscape and contingent charge transport characteristics. The responsivity ( $R$ ) (Figure 1d) and external quantum efficiency (EQE) spectra (Figure S4, Supporting Information) of the OPDs recorded at  $-2$  V are consistent with the optical absorption spectra of the BHJ blends for the different polymers, although their values (Table 1) are somewhat limited by the semi-transparent Ag/ZnS top contact.

We begin our discussion on the relationship between the BHJ characteristics and dark current by noting that  $J_d$  at  $-2$  V shows an exponential correlation with the  $V_{oc}$  of the same devices operating in photovoltaic mode under simulated solar illumination (Figure 2). Since  $J_d$  and  $V_{oc}$  are measured under entirely different illumination and voltage bias conditions, this correlation is intriguing. The  $V_{oc}$  of BHJ photovoltaic devices is known to vary linearly with the energy difference between the acceptor LUMO and donor HOMO,<sup>[17,26]</sup> here referred to as the effective bandgap ( $E_g$ ). Indeed, we find that the  $V_{oc}$  depends linearly on  $E_g$ , with slope of the linear fit equal to 1 (Figure S5, Supporting Information). Hence, the exponential correlation between  $J_d$  and  $V_{oc}$  suggests that the former depends on the effective bandgap  $E_g$ .

**Table 1.**  $J_d$ ,  $R$ , and EQE of BHJ OPDs measured at  $V = -2$  V at photon energy ( $E$ ) for the different polymers.

Polymer	$J_d$ [mA cm <sup>-2</sup> ]	$E$ [eV]	EQE	$R$ [A W <sup>-1</sup> ]
PDPPSDTPS	$1.1 \times 10^{-2}$	1.38	0.16	0.12
PDPP5T	$1.3 \times 10^{-4}$	1.65	0.32	0.20
PDPP3T	$3.5 \times 10^{-5}$	1.42	0.15	0.11
OC <sub>1</sub> C <sub>10</sub> -PPV	$1.1 \times 10^{-6}$	2.34	0.30	0.13
PCDTBT	$1.3 \times 10^{-7}$	2.25	0.35	0.16

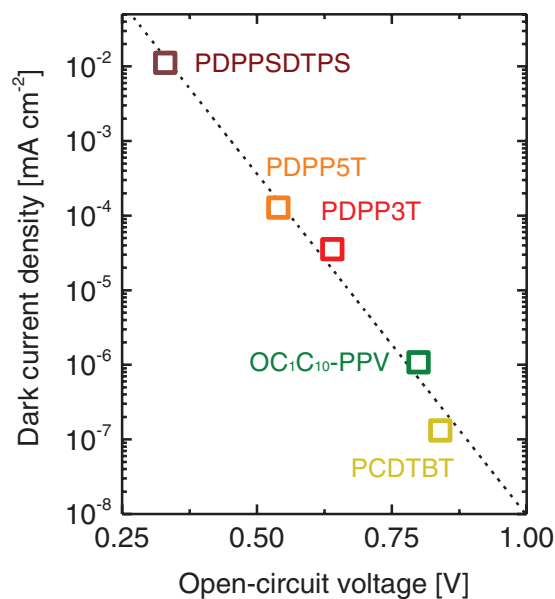


**Figure 2.**  $J_d$  measured at  $V = -2$  V versus the open-circuit voltage measured under simulated solar light (AM1.5G, 100 mW cm<sup>-2</sup>). The dashed line represents an exponential fit to the experimental data.

Further insight into the origin of  $J_d$  can be inferred from the dark current thermal activation energy  $E_a$ , determined from an Arrhenius plot of  $J_d$  against reciprocal temperature (Figure 3). In this experiment,  $J_d$  was measured at each temperature by recording the current density versus time under an applied bias voltage of  $V = -2$  V (Figure S6, Supporting

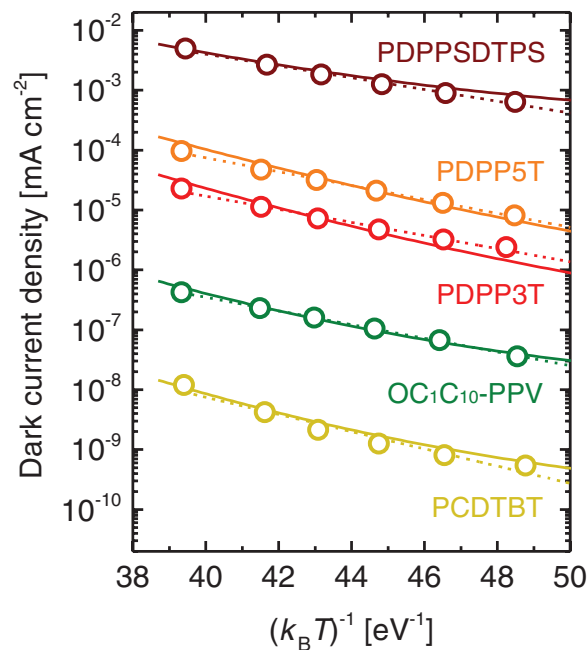


**Figure 3.** Temperature dependence of  $J_d$  at  $V = -2$  V. Empty circles are experimental data. Dashed lines are fits of  $J_d(T)$  to  $J_d \propto \exp(-E_a/k_B T)$ , with  $E_a = 0.22, 0.26, 0.25, 0.26,$  and  $0.28$  eV for PDPPSDTPS, PDPP3T, PDPP5T, OC<sub>1</sub>C<sub>10</sub>-PPV, and PCDTBT, respectively. Solid lines are calculated with Equation (3), as explained in the text.

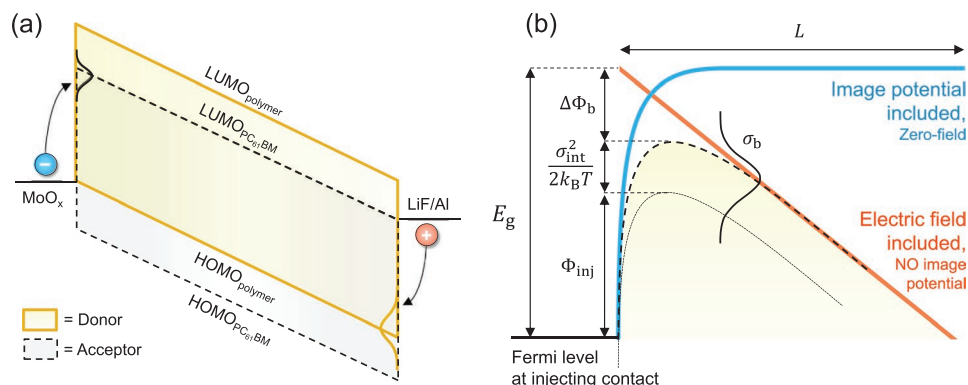


**Figure 4.** a) Schematic of charge injection model. Under reverse bias, electrons are injected from the high work function  $\text{MoO}_x$  electrode into the tail states of the  $\text{PC}_{61}\text{BM}$  LUMO and/or holes are injected from the low work function  $\text{LiF}/\text{Al}$  electrode into the tail states of the polymer HOMO. b) Injection barrier lowering  $\Delta\Phi_b$  due to the image potential under an applied reverse bias for the case of electron injection. The long-dashed curve gives the position of the maximum of the Gaussian distribution of LUMO states. The energetic disorder gives rise to a further injection barrier lowering, leading to an effective value  $\Phi_{\text{inj}}$ .

Information) until a constant value was reached. This procedure eliminates contributions from displacement currents arising from the voltage sweep that become more significant at lower temperatures.  $E_a$  values were obtained from a fit of  $J_d(T)$  to  $J_d \propto \exp(-E_a/k_B T)$ , with  $k_B$  the Boltzmann constant and  $T$  the absolute temperature (dashed lines in Figure 3). The correspondence between the linear fits and the data is not perfect, but does provide a first approximation. Notably, the  $E_a$  values are much lower than any energy difference that can be expected from the HOMO and LUMO levels presented in Figure 1b. Furthermore, the temperature activation of  $J_d$  is very similar for the five OPDs ( $E_a = 0.25 \pm 0.03$  eV), despite the more than five orders of magnitude difference in the absolute values of  $J_d$  near room temperature. Crucially, this comparative invariance in  $E_a$  strongly indicates that bulk thermal generation from the polymer HOMO to the fullerene LUMO cannot be the dominant origin of  $J_d$ , since that would result in  $E_a$  being approximately proportional to  $E_g$ . Below, we show that this unintuitive behavior of the activation energy can be quantitatively explained by considering the influence of energetic disorder on charge injection and transport.

We propose a simple model that relates the temperature dependent magnitude of  $J_d$  to the energy difference between the acceptor LUMO and the donor HOMO. The model assumes that  $\text{Mo}/\text{MoO}_x$  and  $\text{LiF}/\text{Al}$  form Ohmic contacts with the polymer HOMO and the  $\text{PC}_{61}\text{BM}$  LUMO, respectively. It further assumes that continuous donor and acceptor paths exist between the two electrodes. Since bulk thermal generation is demonstrated to be a negligible contributor to  $J_d$  (see Figures S7 and S8, Supporting Information), we assume that the dark current density is primarily due to charge carrier injection from the contacts into the BHJ active layer. We have defined bulk thermal generation as any process that does not require charge injection from the contact layers. This encompasses excitations from the ground state to an excited state on the donor or acceptor, but also excitations to the donor–acceptor charge transfer (CT) state or to sub-bandgap states from which free charges can be generated and collected.<sup>[27]</sup> In fact, bulk thermal generation will be dominated by the latter two possibilities due to their lower transition energies. We note that the internal

quantum efficiency (IQE) has been shown to be independent of whether donor, acceptor, or CT states are excited,<sup>[28]</sup> and thus that additional excitation is generally not required to generate free charge carriers.

In our model, electrons are injected from the high work function  $\text{MoO}_x$  electrode into the tail states of the  $\text{PC}_{61}\text{BM}$  LUMO under reverse bias, while holes are injected from the low work function  $\text{LiF}/\text{Al}$  electrode into the polymer HOMO tail states (Figure 4a). Since both BHJ components are in contact with both electrodes, electron injection and transport will mainly occur via the lowest-energy LUMO (i.e., of the acceptor) and hole injection and transport via the highest-energy HOMO (i.e., of the donor). The work functions of  $\text{MoO}_x$  and  $\text{LiF}/\text{Al}$  can be assumed to align with the top of the Gaussian density of states (DOS) of the donor HOMO and acceptor LUMO, respectively. Under this assumption, the injection barrier is related to the energy difference between the acceptor LUMO and the donor HOMO. We express the reverse bias injection-limited current density as the product of the charge carrier density at the metal–semiconductor interface  $n_{\text{int}}$  and the carrier mobility  $\mu_0$  in the bulk of the active layer:<sup>[29,30]</sup>

$$J_{d,i} = A_i q n_{\text{int},i} \mu_{0,i} F \quad (2)$$

where  $i = e$  for electrons and  $i = h$  for holes,  $A_i$  is a dimensionless factor discussed below, and  $F$  is the effective electric field given by  $F = V/L$ , with  $V$  the applied voltage and  $L$  the active layer thickness. We assume that  $n_{\text{int}}$  at the contacts is established by thermal equilibrium between electrons and holes via an effective injection barrier. When the HOMO and LUMO DOS have a Gaussian shape, the effective injection barrier  $\Phi_{\text{inj}}$  is equal to the effective bandgap  $E_g$  minus a term proportional to the thermal equilibrium energy,  $\left(\frac{\sigma_{\text{int},i}^2}{2k_B T}\right)$ , with  $\sigma_{\text{int},i}$  the

Gaussian DOS width (standard deviation) at the electrode interface.<sup>[31]</sup>  $\Phi_{\text{inj}}$  is further reduced by the image potential barrier lowering<sup>[32]</sup> (Figure 4b), defined as  $\Delta\Phi_b = \sqrt{\frac{qF}{4\pi\epsilon}}$ , with  $\epsilon = \epsilon_0\epsilon_r$  the dielectric permittivity. At sufficiently high electric fields, charge carrier tunneling from the contacts might be possible.



Because the BHJ OPDs are operated at relatively moderate reverse-bias electric fields ( $F \approx 7 \times 10^{-6} \text{ V m}^{-1}$ ), we assume that the hole injection process only occurs into the nearest sites in the polymer, i.e., the sites immediately adjacent to the interface, and likewise that electron injection only occurs into the PC<sub>61</sub>BM sites nearest to the opposite electrode. Under these conditions, the concentration of carriers at the top of the barrier equals  $n_{\text{int},i} = N_{t,i} \exp(-\Phi_{\text{inj}}/k_B T)$  with  $\Phi_{\text{inj}} = E_g - \left(\frac{\sigma_{\text{int},i}^2}{2k_B T}\right) - \Delta\Phi_b$  and with  $N_{t,i}$  the volume density of molecular sites between which the hopping takes place. The mobility  $\mu_{0,i}$  in the zero-field limit and at carrier densities in the independent-particle (Boltzmann) regime is equal to the product of the mobility in the infinite temperature limit,  $\mu_{0,i}^*$ , and a temperature-dependence exponential factor  $\exp\left[-C_i \left(\frac{\sigma_{b,i}}{k_B T}\right)^2\right]$ , where  $\sigma_{b,i}$  is the bulk DOS width and  $C_i \approx 0.4$  within the extended Gaussian disorder model (EGDM).<sup>[33]</sup> Thus, the current density is given by

$$J_{d,i} = A_i q N_{t,i} \exp\left[-\frac{E_g - \left(\frac{\sigma_{\text{int},i}^2}{2k_B T}\right) - \Delta\Phi_b}{k_B T}\right] \cdot \mu_{0,i}^* \exp\left[-C_i \left(\frac{\sigma_{b,i}}{k_B T}\right)^2\right] \cdot \frac{V}{L} \quad (3)$$

The dimensionless prefactor  $A_i$  would be equal to unity for a symmetric device with large injection barriers in which the carrier density is uniform across the active layer thickness.<sup>[31]</sup> Using kinetic Monte-Carlo (KMC) simulations we verified that Equation (3) accurately describes the voltage and temperature dependence of  $J_d$  for symmetric unipolar OPDs when  $\sigma_{\text{int},i} = \sigma_{b,i}$ , with  $A_i$  values of the order of unity (see Figure S9 and Table S1, Supporting Information). We show below that Equation (3) can indeed describe the observed reverse bias dark current densities, albeit using a value of  $\sigma_{\text{int}}$  for holes that is somewhat larger than  $\sigma_b$ .

In the remainder of this work, we use Equation (3) to describe the absolute value and temperature dependence of  $J_d$  for all BHJ OPDs.  $\sigma_{b,i}$ ,  $N_{t,i}$ ,  $\mu_{0,i}^*$ , and  $C_i$  are experimentally determined from the analysis of  $J$ - $V$  characteristics of symmetric unipolar BHJ OPDs using the EGDM (Figures S10–S14, Supporting Information).  $E_g$  (Table 2) is taken as equal to the

energy difference between the PC<sub>61</sub>BM LUMO and the polymer HOMO energies measured with UPS.

Figure 3 shows the calculated  $J_d$  using Equation (3), with  $\sigma_{b,i}$ ,  $N_{t,i}$ ,  $\mu_{0,i}^*$ , and  $C_i$  values as determined from EGDM analysis. We fit the experimental dark current densities using  $E_{g,\text{fit}}$ ,  $\sigma_{\text{int},h}$ , and  $A_{i,\text{fit}}$  as fitting parameters (Table 2). The  $E_{g,\text{fit}}$  values match very well to the expected  $E_g$ , within the experimental error of the UPS data ( $\approx 0.1 \text{ eV}$ ).<sup>[17]</sup> We found that when  $\sigma_{\text{int}}$  was set equal to  $\sigma_b$ , the experimental activation barriers would not be reproduced correctly. However, a slight increase of  $\sigma_{\text{int}}$  for holes compared to  $\sigma_b$  resulted in good experimental correspondence. In Figure S15 (Supporting Information) we show that for all BHJ systems a much larger increase of  $\sigma_{\text{int}}$  for electrons would be required to obtain good agreement with the experimental data. This indicates that broadening the DOS width of the HOMO at the interface is more likely to determine the experimental  $J_d$ . Optimal fitting of the experimental data was obtained using the  $\sigma_{\text{int},h}$  values in Table 2 for holes, while keeping  $\sigma_{\text{int},e} = \sigma_{b,e}$ . We note that the optimal  $\sigma_{\text{int},h}$  values are proportional to and systematically higher than  $\sigma_{b,h}$  (by a common factor of  $\approx 1.4$ ), possibly indicating a broadening of the DOS at the interface between the active layer and the LiF/Al top contact. This effect was modeled using KMC simulations (Figure S16, Supporting Information). The KMC simulations predict a larger effective DOS width for holes near the low work function electrode due to the high density of electrons at the metal contact, enhancing hole injection into the polymer HOMO, and vice versa for the electrons near the high work function electrode. Notably,  $A_i$  values were found in each polymer to be of the order of  $10^{-3}$ , i.e., much lower than the theoretical value of unity, for both electrons and holes. Although at present we are unable to offer a definitive explanation, we propose three possible reasons for the current reduction: charges captured by trap states not contributing to  $J_d$ , the applied model not fully accounting for the image potential, and spatially inhomogeneous charge injection due to the filamentary BHJ energetic landscape.

To ascertain the wider applicability of our model, we characterized the energetic disorder and the charge carrier mobility of pure polymer films, as opposed to the BHJ films discussed above (Figures S17 and S18, Supporting Information). We found that both  $\sigma_{b,h}$  and  $\mu_{0,h}$  at room temperature change drastically

**Table 2.** Hole and electron disorder parameter  $\sigma_{b,i}$  in the bulk of the active layer, volume density of molecular sites  $N_{t,i}$ , zero-field, zero-carrier density mobility  $\mu_{0,i}^*$  in the infinite temperature limit, and  $C_i$  parameter all as determined from EGDM analysis on single carrier BHJ OPDs.  $E_g$  is the effective bandgap as determined from UPS measurements.  $E_{g,\text{fit}}$ ,  $\sigma_{\text{int},h}$ , and  $A_{i,\text{fit}}$  are the effective bandgap, disorder parameter for holes at the interface, and prefactor used to fit experimental data in Figure 3, respectively.

Polymer	Parameters from EGDM analysis									Fitting parameters		
	$\sigma_{b,h}$ [eV]	$\sigma_{b,e}$ [eV]	$N_{t,h}$ [ $10^{27} \text{ m}^{-3}$ ]	$N_{t,e}$ [ $10^{27} \text{ m}^{-3}$ ]	$\mu_{0,h}^*$ [ $\text{m}^2 \text{ V}^{-1} \text{ s}^{-1}$ ]	$\mu_{0,e}^*$ [ $\text{m}^2 \text{ V}^{-1} \text{ s}^{-1}$ ]	$C_h$	$C_e$	$E_g$ [eV]	$E_{g,\text{fit}}$ [eV]	$\sigma_{\text{int},h}$ [eV]	$A_{i,\text{fit}}$ [ $10^{-3}$ ]
PDPPSDTPS	0.10	0.07	1.0	1.0	$2.7 \times 10^{-5}$	$1.5 \times 10^{-5}$	0.38	0.38	0.80	0.80	0.14	0.5
PDPP5T	0.09	0.07	1.0	1.0	$1.2 \times 10^{-5}$	$1.1 \times 10^{-5}$	0.37	0.35	0.86	0.83	0.13	0.5
PDPP3T	0.10	0.07	1.0	1.0	$7.9 \times 10^{-5}$	$8.0 \times 10^{-6}$	0.35	0.35	1.03	0.97	0.14	0.5
OC <sub>1</sub> C <sub>10</sub> -PPV	0.12	0.07	0.2	1.0	$2.9 \times 10^{-5}$	$5.9 \times 10^{-6}$	0.35	0.35	1.08	1.16	0.17	2.5
PCDTBT	0.125	0.08	0.25	1.0	$7.1 \times 10^{-6}$	$6.2 \times 10^{-5}$	0.35	0.35	1.28	1.26	0.176	2.0

when compared to the blend due to the absence of PC<sub>61</sub>BM (Table S2, Supporting Information).<sup>[34]</sup> In addition, the changes in  $\sigma_{b,h}$  and  $\mu_{0,h}$  at room temperature are strongly dependent on the specific polymer. Therefore, studying the energetic disorder and the carrier concentration dependent mobility function in the pure polymer is less relevant to understand the dark current of BHJ OPDs. Furthermore, we calculated the voltage dependence of  $J_d$  at room temperature for all BHJ OPDs using our model, as shown in Figure S19 (Supporting Information). The model can relatively well explain the voltage dependence at moderately high bias ( $-2.5 \text{ V} < V < -0.5 \text{ V}$ ) but is less accurate at lower bias ( $-0.5 \text{ V} < V < 0 \text{ V}$ ). This might be due to an inadequate description of the injection process at very low electric fields.

Additionally, we note that the experimental temperature dependence of  $J_d$  at  $V = -2 \text{ V}$  is comparable to that of the hole-only current density (Figure S20, Supporting Information). In our model, the reverse bias dark current density is dominated by hole injection into the tail states of the polymer HOMO for all BHJ systems, due the higher value of  $\sigma_{int,h}$  compared to  $\sigma_{int,e} = \sigma_{b,e}$ . It is likely that this corresponds to the actual situation, as Figure S15 (Supporting Information) shows that relatively large changes in  $\sigma_{int,e}$  would be required to reach agreement with experiment. Equation (3) provides insight into the temperature dependence of the activation energy via

$$E_a = \frac{d \ln(J_d)}{d\left(\frac{1}{k_B T}\right)} \approx E_g + \frac{1}{k_B T} (2C_h \sigma_{b,h}^2 - \sigma_{int,h}^2) - \Delta\Phi_b \quad (4)$$

The second term in the right-hand part of this expression is negative, as  $2C_h \approx 0.75$  and  $\sigma_{int,h}^2 \approx 2\sigma_{b,h}^2$ . Equation (4) explains how the lower than anticipated activation energies of  $J_d$  are based on the reduction of the effective injection barrier due to the Gaussian energetic disorder. Furthermore, it successfully describes how  $E_a$  decreases at lower temperatures, as shown in Figure S21 (Supporting Information). Notably,  $E_a$  depends on the image potential barrier lowering  $\Delta\Phi_b$  and thus it is expected to decrease with increasing reverse bias voltage. The agreement between Equation (4) and  $E_a$  measured at different bias voltages might be an interesting subject of further research.

Finally, from the measured unipolar  $J$ - $V$  curves of devices with Ohmic contacts (Figures S10–S14, Supporting Information) it may be expected that for the materials studied the dark current density under forward bias ( $V = +2 \text{ V}$ ) is determined almost completely by the electron contribution. Quantitatively, such a conclusion would also follow from the ratio

$$\text{of the EGDM mobility } \mu_{0,i}^* \exp\left[-C_i \left(\frac{\sigma_{b,i}}{k_B T}\right)^2\right] \text{ for electrons and}$$

holes in the Boltzmann regime, which provides the relevant comparison for these rather thick ( $\approx 280 \text{ nm}$ ) devices for the relatively low voltage used. For PCDTBT, e.g., the electron:hole mobility ratio (from Table 2) in this regime at 298 K is approximately equal to 1200. Consistent with this view, Figure S20 (Supporting Information) shows that under forward bias the temperature dependence of  $J_d$  is identical to that of the electron mobility in the Boltzmann regime. Thus, the current density in forward bias is mainly dominated by electron transport

via PC<sub>61</sub>BM, in line with previously reported observations for polymer:fullerene BHJ solar cells.<sup>[35,36]</sup>

In conclusion, for five different polymer:PC<sub>61</sub>BM photodiodes we find that the dark current density under reverse bias correlates exponentially with the  $V_{oc}$  of the same devices under simulated solar light. This confirms the expected scaling of  $J_d$  with the effective bandgap of the semiconducting active layer. However, the temperature dependence of  $J_d$  reveals activation energies much smaller than the effective bandgap. The magnitude of  $J_d$  and its activation energy can be described quantitatively by including the effect of Gaussian energetic disorder of the organic semiconductor on the injection and transport of electrons and holes. In addition, the low and approximately invariant  $E_a$  values ( $\approx 0.25 \text{ eV}$ ) for each polymer indicate that the dark current is predominantly due to injection and transport of carriers via low energy sites in the disordered semiconductor, rather than thermal excitation of carriers across the electronic gap. In the five polymer-fullerene OPDs, the reverse bias  $J_d$  is dominated by hole current because of the higher energetic disorder of the polymer compared to the fullerene acceptor, which results in a lower barrier for hole injection compared to electron injection. Under forward bias, no appreciable barriers for charge injection exist and then  $J_d$  is dominated by the electron current, because the electron mobility is higher than the hole mobility. Further reduction of the dark current, and thus improvement of OPD detectivity at a given photon energy, may thus be achieved by reducing the energetic disorder of the organic semiconductors,<sup>[10]</sup> or by otherwise reducing injection of carriers under reverse bias.<sup>[5,11,12]</sup>

## Experimental Section

**Ultraviolet Photoelectron Spectroscopy:** The UPS measurements were performed according to recently published methods<sup>[17]</sup> and are further detailed in the Supporting Information.

**OPD Fabrication:** A 100 nm molybdenum film was sputtered on glass and subsequently patterned using photolithography to form the bottom electrode. Next, a thin film of insulating photoresist was processed to cover the perimeter of the Mo bottom electrode (Figure S2, Supporting Information), thereby minimizing undesirable current leakage paths. Prior to spin coating of the polymer:PC<sub>61</sub>BM blend the substrates were cleaned and treated with O<sub>2</sub> plasma for 3 min, leading to the formation of a thin MoO<sub>x</sub> layer. PDPPSDTPS ( $M_n = 50 \text{ kg mol}^{-1}$ ) was blended with PC<sub>61</sub>BM 1:2 (w/w) in a chloroform solution with 5 vol% o-dichlorobenzene at 6 mg mL<sup>-1</sup> polymer concentration. PDPP5T ( $M_n = 40 \text{ kg mol}^{-1}$ ) was blended with PC<sub>61</sub>BM 1:2 (w/w) in a chloroform solution with 10 vol% o-dichlorobenzene at 9 mg mL<sup>-1</sup> polymer concentration. PDPP3T ( $M_n = 60 \text{ kg mol}^{-1}$ ) was blended with PC<sub>61</sub>BM 1:2 (w/w) in a chloroform solution with 7.5 vol% o-dichlorobenzene at 7 mg mL<sup>-1</sup> polymer concentration. OC<sub>1</sub>C<sub>10</sub>-PPV ( $M_n = 350 \text{ kg mol}^{-1}$ ) and PCDTBT ( $M_n = 60 \text{ kg mol}^{-1}$ ) were blended with PC<sub>61</sub>BM 1:4 (w/w) in a chlorobenzene solution at 10 and 9 mg mL<sup>-1</sup> polymer concentration, respectively. The polymer:PC<sub>61</sub>BM blends were cast by spin coating at 750 rpm in a N<sub>2</sub>-filled glove box resulting in a  $\approx 280 \text{ nm}$  layer. The active layers were dried overnight in a vacuum chamber at  $\approx 6 \times 10^{-7}$  mbar and the OPDs were finished with evaporated LiF (1 nm), Al (1.5 nm), Ag (10 nm), and ZnS (30 nm). The OPD active area was 2 mm × 2 mm.

**OPD Characterization:**  $J$ - $V$  characteristics in dark conditions were measured with a probe station in a N<sub>2</sub>-filled glove box, sweeping the voltage from -2 to +2 V and back, using a slow scan speed of 0.05 V s<sup>-1</sup> to minimize displacement currents. To determine the dark current density at different temperatures,  $J_d$  was measured in a cryostat under vacuum versus time at a constant applied bias of -2 V until a constant value was reached.

The open-circuit voltage of each OPD analyzed in this work was recorded in a N<sub>2</sub>-filled glove box under simulated solar light using a tungsten-halogen lamp coupled to a UV filter and daylight filter (Hoya LB120). The EQE setup was based on a tungsten-halogen lamp, a chopper, a monochromator (Oriel, Cornerstone 130), a preamplifier (Stanford Research Systems SR570), and a lock-in amplifier (Stanford Research Systems SR830 DSP). The active area for EQE measurements was defined by a circular aperture of 1 mm in diameter. Sub-bandgap EQE spectra were acquired by irradiating each OPD with monochromatic light (Oriel Cornerstone 260) (10 nm band width, modulated at 330 Hz). The sensitivity was enhanced using a preamplifier (Stanford Research Systems SRS500, also used to apply a -2 V bias) and a lock-in amplifier (Stanford Research Systems SRS830). The subgap EQE spectra were corrected for the illumination intensity (determined from calibrated Si and InGaAs photodiodes), and then scaled to EQE values determined in the main absorption band.

## Supporting Information

Supporting Information is available from the Wiley Online Library or from the author.

## Acknowledgements

The research received funding from the Ministry of Education, Culture and Science (Gravity program 024.001.035) and the European Research Council under the European Union's Seventh Framework Programme (FP/2007-2013)/ERC Grant Agreement No. 339031. M.D. thanks the Marie Skłodowska-Curie Actions Innovative Training Network "H2020-MSCA-ITN-2014 INFORM – 675867" for the financial support. The authors would like to thank the process engineers of Holst Centre's R&D Pilot Line for the fabrication of the OPD substrates.

## Conflict of Interest

The authors declare no conflict of interest.

## Keywords

bulk heterojunction, charge injection, dark current, organic photodiodes, reverse bias

Received: September 17, 2019

Revised: October 5, 2019

Published online:

- [1] R. D. Jansen-van Vuuren, A. Armin, A. K. Pandey, P. L. Burn, P. Meredith, *Adv. Mater.* **2016**, *28*, 4766.  
 [2] K. Baeg, M. Binda, D. Natali, M. Caironi, Y. Noh, *Adv. Mater.* **2013**, *25*, 4267.  
 [3] Y. S. Rim, S. Bae, H. Chen, N. De Marco, Y. Yang, *Adv. Mater.* **2016**, *28*, 4415.  
 [4] M. Kiehl, O. Dhez, G. Pecastaings, A. Curutchet, L. Hirsch, *Sci. Rep.* **2016**, *6*, 39201.  
 [5] X. Zhou, D. Yang, D. Ma, *Adv. Opt. Mater.* **2015**, *3*, 1570.  
 [6] X. Liu, H. Wang, T. Yang, W. Zhang, X. Gong, *ACS Appl. Mater. Interfaces* **2012**, *4*, 3701.  
 [7] Y. Fang, A. Armin, P. Meredith, J. Huang, *Nat. Photonics* **2019**, *13*, 1.  
 [8] G. H. Gelinck, A. Kumar, D. Moet, J. P. J. Van Der Steen, A. J. J. M. Van Breemen, S. Shanmugam, A. Langen, J. Gilot, P. Groen, R. Andriessen, M. Simon, W. Ruetten, A. U. Douglas,

- R. Raaijmakers, P. E. Malinowski, K. Myny, *IEEE Trans. Electron Devices* **2016**, *63*, 197.  
 [9] A. H. Fallahpour, S. Kienitz, P. Lugli, *IEEE Trans. Electron Devices* **2017**, *64*, 2649.  
 [10] H. Shekhar, O. Solomeshch, D. Liraz, N. Tessler, *Appl. Phys. Lett.* **2017**, *111*, 223301.  
 [11] S. Valouch, C. Hönes, S. W. Kettlitz, N. Christ, H. Do, M. F. G. Klein, H. Kalt, A. Colsmann, U. Lemmer, *Org. Electron.* **2012**, *13*, 2727.  
 [12] P. E. Keivanidis, P. K. H. Ho, R. H. Friend, N. C. Greenham, *Adv. Funct. Mater.* **2010**, *20*, 3895.  
 [13] J. B. Park, J. W. Ha, S. C. Yoon, C. Lee, I. H. Jung, D. H. Hwang, *ACS Appl. Mater. Interfaces* **2018**, *10*, 38294.  
 [14] M. R. Esopi, M. Calcagno, Q. Yu, *Adv. Mater. Technol.* **2017**, *2*, 1700025.  
 [15] W. Wang, F. Zhang, M. Du, L. Li, M. Zhang, K. Wang, Y. Wang, B. Hu, Y. Fang, J. Huang, *Nano Lett.* **2017**, *17*, 1995.  
 [16] J. Miao, F. Zhang, *Laser Photonics Rev.* **2019**, *13*, 1800204.  
 [17] R. E. M. Willems, C. H. L. Weijtens, X. de Vries, R. Coehoorn, R. A. J. Janssen, *Adv. Energy Mater.* **2019**, *9*, 1803677.  
 [18] H. Yoshida, *J. Phys. Chem. C* **2014**, *118*, 24377.  
 [19] K. H. Hendriks, W. Li, M. M. Wienk, R. A. J. Janssen, *J. Am. Chem. Soc.* **2014**, *136*, 12130.  
 [20] M. Li, J. Li, D. Di Carlo Rasi, F. J. M. Colberts, J. Wang, G. H. L. Heintges, B. Lin, W. Li, W. Ma, M. M. Wienk, R. A. J. Janssen, *Adv. Energy Mater.* **2018**, *8*, 1800550.  
 [21] J. J. van Franeker, M. Turbiez, W. Li, M. M. Wienk, R. A. J. Janssen, *Nat. Commun.* **2015**, *6*, 6229.  
 [22] J. K. J. van Duren, X. Yang, J. Loos, C. W. T. Bulle-Lieuwma, A. B. Sieval, J. C. Hummelen, R. A. J. Janssen, *Adv. Funct. Mater.* **2004**, *14*, 425.  
 [23] V. S. Gevaerts, A. Furlan, M. M. Wienk, M. Turbiez, R. A. J. Janssen, *Adv. Mater.* **2012**, *24*, 2130.  
 [24] S. Dongaonkar, J. D. Servaites, G. M. Ford, S. Loser, J. Moore, R. M. Gelfand, H. Mohseni, H. W. Hillhouse, R. Agrawal, M. A. Ratner, T. J. Marks, M. S. Lundstrom, M. A. Alam, *J. Appl. Phys.* **2010**, *108*, 124509.  
 [25] P. Kaienburg, P. Hartnagel, B. E. Pieters, J. Yu, D. Grabowski, Z. Liu, J. Haddad, U. Rau, T. Kirchartz, *J. Phys. Chem. C* **2018**, *122*, 27263.  
 [26] V. D. Mihailtchi, P. W. M. Blom, J. C. Hummelen, M. T. Rispens, *J. Appl. Phys.* **2003**, *94*, 6849.  
 [27] B. Bouthinon, R. Clerc, J. Vaillant, J. Verilhac, J. Faure-Vincent, D. Djurado, I. Ionica, G. Man, A. Gras, G. Pananakakis, R. Gwoziecki, A. Kahn, *Adv. Funct. Mater.* **2015**, *25*, 1090.  
 [28] K. Vandewal, S. Albrecht, E. T. Hoke, K. R. Graham, J. Widmer, J. D. Douglas, M. Schubert, W. R. Mateker, J. T. Bloking, G. F. Burkhard, A. Sellinger, J. M. J. Fréchet, A. Amassian, M. K. Riede, M. D. McGehee, D. Neher, A. Salleo, *Nat. Mater.* **2014**, *13*, 63.  
 [29] J. G. Simmons, *Phys. Rev. Lett.* **1965**, *15*, 967.  
 [30] T. van Woudenberg, P. W. M. Blom, M. C. J. M. Vissenberg, J. N. Huiberts, *Appl. Phys. Lett.* **2001**, *79*, 1697.  
 [31] J. J. M. van der Holst, M. A. Uijtewaal, B. Ramachandran, R. Coehoorn, P. A. Bobbert, G. A. de Wijs, R. A. de Groot, *Phys. Rev. B* **2009**, *79*, 085203.  
 [32] V. I. Arkhipov, U. Wolf, H. Bässler, *Phys. Rev. B* **1999**, *59*, 7514.  
 [33] W. F. Pasveer, J. Cottaar, C. Tanase, R. Coehoorn, P. A. Bobbert, P. W. M. Blom, D. M. de Leeuw, M. A. J. Michels, *Phys. Rev. Lett.* **2005**, *94*, 206601.  
 [34] V. D. Mihailtchi, L. J. A. Koster, P. W. M. Blom, C. Melzer, B. de Boer, J. K. J. van Duren, R. A. J. Janssen, *Adv. Funct. Mater.* **2005**, *15*, 795.  
 [35] G. A. H. Wetzelaer, M. Kuik, M. Lenes, P. W. M. Blom, *Appl. Phys. Lett.* **2011**, *99*, 153506.  
 [36] J. K. J. van Duren, V. D. Mihailtchi, P. W. M. Blom, T. van Woudenberg, J. C. Hummelen, M. T. Rispens, R. A. J. Janssen, M. M. Wienk, *J. Appl. Phys.* **2003**, *94*, 4477.